Journal of Science and Technology – Engineering and Technology for Sustainable Development
Volume 36, Issue 5, November 2026, 044–052

Synthesis of Nanoscale Ag@ZnO Materials and Evaluation of Methylene Blue Degradation Ability under Ultraviolet and Visible Light

Hoa Lai Tien[1,2], Mai Nguyen Thi Tuyet[2,*], Dung Ta Ngoc[2], Chinh Huynh Dang[2], Anh Luu Thi Lan[1]

[1]*Faculty of Engineering Physics, Hanoi University of Science and Technology, Ha Noi, Vietnam*
[2]*School of Chemistry and Life Sciences, Hanoi University of Science and Technology, Ha Noi, Vietnam*
[*]*Corresponding author email: mai.nguyenthituyet@hust.edu.vn*

Abstract

As is known, traditional treatment methods often struggle with the efficient degradation of organic dyes, creating an urgent need for advanced and sustainable materials in wastewater treatment. In this study, Dicliptera tinctoria leaf extract was used to synthesize a green Ag@ZnO nanomaterial, and the optimal Ag mixing level was investigated to achieve superior photocatalytic performance under both UV and visible light. Additionally, the feasibility and interbatch stability of the material were systematically evaluated. The crystalline phase and optical structural properties of the synthesized material were characterized by X-ray diffraction (XRD), diffuse reflectance spectroscopy (DRS), and UV-Vis absorption spectroscopy. The results indicate that the studied parameters significantly influenced the degradation efficiency of Methylene B*lue* (MB). *When water was used as the solvent during the extraction process, the degradation efficiency of MB reached a maximum of 91.11% after 90 minutes of UV irradiation. Using a 1:1 mixture of water and alcohol, the degradation efficiency improved notably, reaching 100% after only 60 minutes of UV irradiation. Varying the concentration of the MB dye also affects its degradation efficiency; specifically, reducing the dye concentration leads to an increase in degradation efficiency. The optical property analysis indicates that at an MB concentration of 5 ppm, a remarkable degradation efficiency of 98.12% is achieved under visible light irradiation over a reaction period of 180 minutes in order to ensure complete evaluation.*

Keywords: Ag@ZnO NsMs, *Dicliptera tinctoria*, green synthesis, photocatalysis, UV-Vis.

1. Introduction

Industrial dye pollution poses a critical threat, with Methylene Blue (MB) chosen as the model pollutant due to its high persistence and toxicity. Traditional methods -such as adsorption (phase transfer only), chemical treatments (hazardous sludge and high costs), and biological processes (long retention times) -fall short. MB serves as an ideal probe for wastewater remediation due to its stable aromatic structure and strong interaction with catalyst surfaces. Advanced nano Ag@ZnO photocatalysts overcome these limitations via surface plasmon resonance and reactive oxygen species generation. This system effectively mineralizes MB into harmless CO_2 and H_2O under light irradiation [1–4]. Green synthesis has emerged as a promising approach due to its environmental friendliness, simplicity, cost-effectiveness, and high photocatalytic efficiency. For instance, Kumar *et al*. [5] synthesized ZnO using Ambrosia ambrosioides leaf and root extracts, achieving degradation efficiencies of MB, Methyl orange (MO), Congo red (CR), and Methyl red (MR) under ultraviolet (UV) light of 90% after 60 min, 100 min, 60 min, and 140 min, respectively. Patel *et al.* [6] green-synthesized CuO from Seriphidium Oliverianum leaf extract, achieving degradation of Methyl green (MG) and Methyl orange (MO) under sunlight, reaching 65% after 60 minutes.

In this study, we synthesized Ag@ZnO using a green method with extracts from *Dicliptera tinctoria* (DT), which has rarely been reported. The DT leaf extract contains anthocyanins, flavonoids, and chlorophyll, which act as reducing and stabilizing agents in the synthesis of Ag-doped ZnO (Ag@ZnO). Moreover, it effectively controls the size and uniformity of the synthesized nanoparticles [7, 8]. The objective of this study is to determine the optimal Ag doping concentration that leads to the highest degradation efficiency. Ag doping helps broaden the surface plasmon resonance range, enabling the material to perform effectively under visible light.

2. Chemicals and Experimental Procedures

2.1. Chemicals

The chemicals used included *Dicliptera tinctoria* leaf powder (local market, Vietnam), Zinc nitrate hexahydrate ($Zn(NO_3)_2{\cdot}6H_2O$, 99%, AR-China), Silver nitrate ($AgNO_3$, 99.8%, AR-China). MB dye ($C_{16}H_{18}ClN_3S$, 95%, Sigma-Aldrich), and Distilled water.

p-ISSN 3093-3242
e-ISSN 3093-3579
https://doi.org/10.51316/jst.195.etsd.2026.36.5.6
Received: Dec 31, 2025; Revised: Jan 14, 2026;
Accepted: Aug 27, 2026; Online: Oct 29, 2026

2.2. Dicliptera tinctoria Leaves Extraction Procedure

Fig. 1 illustrates the extraction scheme of *Dicliptera tinctoria* extract from *Dicliptera tinctoria* powder. A beaker containing 75 mL of distilled water was prepared, and then 2 g of *Dicliptera tinctoria* leaves powder was added. The mixture was stirred and heated at 80 °C for 1 hour. After the process, the resulting mixture contained organic compounds from *Dicliptera tinctoria*. The mixture was then filtered using Whatman filter paper to remove the solid residues, yielding the *Dicliptera tinctoria* extract solution.

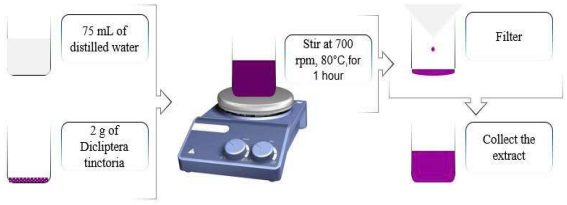


Fig. 1. *Dicliptera tinctoria* extraction scheme

2.3. Synthesis Procedure of Ag@ZnO NsMs

Fig. 2 shows the schematic diagram of the Ag@ZnO NsMs synthesis from $Zn(NO_3)_2$ and $AgNO_3$ precursors.

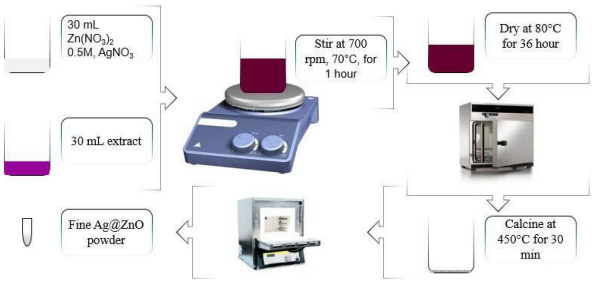


Fig. 2. Green synthesis Scheme of Ag@ZnO NsMs

Table 1. Investigation of parameters affecting the properties of nanoscale Ag@ZnO materials.

Sample	Value	Investigated parameter
H31		Non – calcined sample
H34	1%	+Molar ratio of Ag^+ doped into ZnO; +Non alcohol (only distilled water is used as the solvent).
H35	3%	
H36	5%	
H37	7%	
H38	10%	
H39	1 : 1	+Use alcohol - water ratio in the extract; +(Repeated alcohol - to - water ratio in the extract for testing the replicate sample.
H40	1 : 1	
H41	1 : 1	

A solution mixture containing 30 mL of $Zn(NO_3)_2$ and $AgNO_3$ was mixed with 60 mL of the previously prepared extract and stirred with heating at 70 °C for 1 hour. The mixture was then dried at 80 °C for 36 hours, yielding a Ag@ZnO solid containing organic impurities. The solid sample was subsequently calcined at 450 °C for 30 minutes to remove impurities, resulting in Ag@ZnO nanoparticles (nanoscale Ag@ZnO materials - Ag@ZnO NsMs).

In Table 1 above, our research group investigated samples with several parameters affecting the materials characterizations and photocatalytic efficiency, including: stirring temperature, calcination time, and calcination temperature. The aim was to determine the optimal conditions for the materials synthesis process.

2.4. Photocatalytic Experimental Procedure

In this experiment, 20 mg of Ag@ZnO was added to 50 mL of MB dye solution with a concentration of 5 ppm. The experimental system was stirred in complete darkness for 60 minutes to reach adsorption equilibrium. Every 30 minutes, 5 mL of the solution was withdrawn for analysis using UV-Vis spectroscopy. Subsequently, the mixture was irradiated with a 250/300W Osram Ultra lamp (emitting in the UVA-UVB region) and every 30 minutes, 5 mL of the solution was collected for UV-Vis analysis.

Visible light irradiation was carried out using a 250 W, 220V Osram lamp.

2.5. Materials Characterization

The characterizations of the materials were investigated using the following measurement methods: X-ray diffraction (XRD, X'pert Pro) method with Cu-Kα radiation (λ= 1.54065 Å), scan rate 0.03°/2 s, scan angle $2\theta \approx$ 25–80°. Diffuse Reflectance Spectroscopy (DRS, JASCO V-750 with 60 mm integrated sphere, scan rate 200 nm/min) method, this provides information on the emission or absorption according to wavelengths or the bandgap energy (Eg) of the materials. The UV-Vis spectra measurement (DR3900-Hach spectrophotometer), this technique used to investigate the photocatalytic performance of the photocatalysis materials with MB dye solution.

3. Results and Discussion

3.1. The Effect of Ag Ions Doping on Material Characterizations

With the aim of improving the photocatalytic efficiency of the material, in this study, the element Ag derived from the precursor $AgNO_3$ was selected to dope into the materials, thereby potentially enhancing the properties of the synthesized materials.

3.1.1. Reasons for choosing Ag as a dopant

In fact, ZnO has a bandgap energy of around 3.37 eV, meaning that this ZnO nanomaterial only strongly absorbs

energy in the near-ultraviolet region (around 380 nm) [5]. Also, with the aim of enabling the material to efficiently operate under visible light, a suitable doping element was selected. Among them, Ag stands out as a prominent dopant, acting as a charge trap due to its good electrical conductivity, which slows down the recombination of electrons and holes in ZnO. This leads to a longer electron - hole lifetime, resulting in improved photocatalytic performance. In addition, Ag exhibits a strong surface plasmon effect in the visible wavelength range of approximately 400 - 600 nm, which benefits the dye degradation process. Moreover, Ag helps generate additional active sites for the formation of $\bullet O_2^-$ and •OH radicals [4, 9].

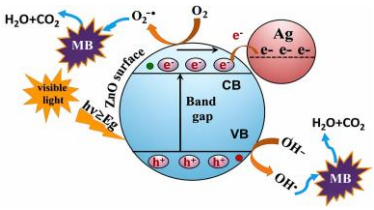


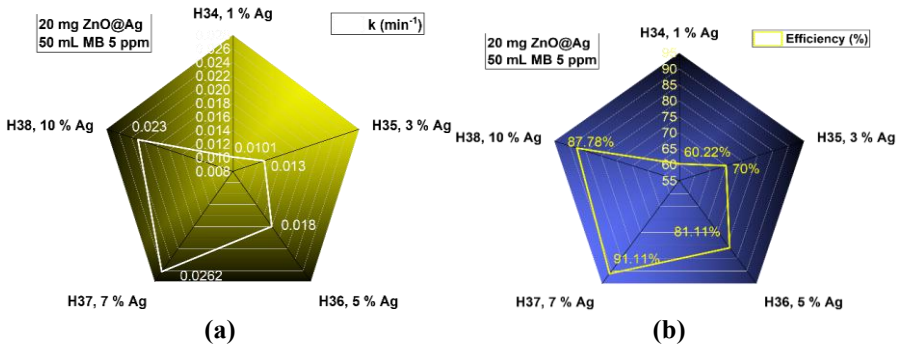
Fig. 3. The diagram illustrates the photocatalytic mechanism of the Ag-doped ZnO nanoparticles [9]

Fig. 3 illustrates the photocatalytic degradation mechanism of MB dye by Ag-doped ZnO nanoparticles under visible light irradiation [9]. Under light illumination, electrons in the valence band (VB) of ZnO are excited to the conduction band (CB), leaving holes in the VB. Due to the lower Fermi level of Ag, which acts as an electron sink, photogenerated electrons rapidly transfer from ZnO to Ag, effectively suppressing electron-hole recombination. This prolonged charge separation facilitates the generation of reactive oxygen species, such as $\bullet O_2^-$ (from electrons reacting with O_2) and •OH (from holes reacting with H_2O/OH^-), which possess strong oxidation capabilities to decompose the dye. Additionally, the surface plasmon resonance (SPR) effect of Ag broadens the light absorption range, enabling the Ag-doped ZnO nanoparticles to efficiently absorb visible light. Here, the Ag dopant concentrations in the ZnO nanoparticles, calculated based on the molar ratio of the Zn precursor, were 1%, 3%, 5%, 7%, and 10%, corresponding to the five samples H34, H35, H36, H37, and H38, respectively.

3.1.2. Photocatalytic analysis

Fig. 4a shows the plot of $\ln(C_0/C)$ reflecting the reaction rate constant k for the five samples H34, H35, H36, H37, and H38, which are 0.0101 min^{-1}, 0.013 min^{-1}, 0.018 min^{-1}, 0.0262 min^{-1}, and 0.023 min^{-1}, respectively. From this, it can be seen that the k value of sample H37 is the highest, indicating the best reaction efficiency among the selected samples and suggesting that this $AgNO_3$ doping ratio is optimal for Ag@ZnO NsMs synthesis. Fig. 4b presents the MB degradation efficiency of samples H34, H35, H36, H37, and H38 after 90 minutes of UV irradiation. The efficiencies are 60.22%, 70%, 81.11%, 91.11%, and 87.78%, respectively. Compared to the best undoped sample H31 (84.95%), these results demonstrate a superior MB degradation performance. The highest efficiency of 91.11% indicates that the optimal Ag doping ratio in Ag@ZnO is 7%. Lower efficiencies of samples H34, H35, and H36 suggest that a small amount of Ag is insufficient to form an effective Schottky barrier due to low presence and poor dispersion. Additionally, shallow trap levels may cause electrons to recombine with holes, reducing photocatalytic performance. Moreover, low Ag content can partially block active sites on ZnO [10]. For sample H37, the Ag content is sufficient to form an effective Schottky barrier and induce a strong surface plasmon effect in the visible range. At this level, Ag acts as an electron sink, reducing electron - hole recombination and enhancing photocatalytic activity. For sample H38, the slight decrease in efficiency is likely due to excessive Ag coverage, which can shield ZnO active sites and reduce its UV - driven photocatalytic performance.

Therefore, a 7% Ag doping ratio in Ag@ZnO enhances the photocatalytic performance by increasing the surface plasmon effect in the visible range, reducing electron - hole recombination, and increasing the effective surface area.



(a) **(b)**

Fig. 4. The UV-Vis results for (a) the reaction rate and (b) degradation efficiency of 5 ppm MB under UV light after 90 minutes for Ag@ZnO NsMs samples. Here, investigating the effect of Ag doping concentration (based on the Ag molar ratio to Zn), are shown for samples H34 (1% Ag), H35 (3% Ag), H36 (5% Ag), H37 (7% Ag), H38 (10% Ag)

3.2. Effect of Dicliptera Tinctoria Extract at the Optimized Water: Ethanol Ratio

In this investigation part, two types of Dicliptera tinctoria extracts were studied: one prepared with water only, corresponding to sample H37, and the other prepared with a water : ethanol mixture at a 1 : 1 ratio (the optimized ratio reported in previous studies of our group), corresponding to sample H39.

3.2.1. X-ray diffraction result

Fig. 5 shows the XRD patterns of sample H31 (ZnO without Ag doping), sample H37, and sample H39. All samples were fully crystallized with a hexagonal wurtzite structure. The main diffraction peaks of the hexagonal ZnO phase appeared at 2θ≈ 31.8°, 34.4°, 36.3°, 47.5°, 56.6°, 62.8°, 66.3°, 67.9°, and 69.1°, corresponding to the (100), (002), (101), (102), (110), (103), (200), (112), and (201) crystal planes according to the JCPDS 01-079-0206 standard [11]. The XRD diffraction peaks of the face-centered cubic (fcc) Ag phase appeared at 2θ≈ 27.8°, 32.2°, 38.1°, 44.3°, 46.2°, 54.8°, 57.4°, 64.4°, and 77.4°, corresponding to the (210), (122), (111), (200), (231), (142), (241), (220), and (311) crystal planes according to the JCPDS 04-0783 standard [12]. Compared with sample H31, the diffraction peaks of sample H37 are less sharp, indicating a reduced crystallinity of the material. This may be attributed to the fact that during the synthesis of Ag@ZnO, Ag^+ ions tend to pair with OH^- ions and subsequently decompose into Ag_2O according to the following reaction:

$$Ag^+ + 2OH^- \rightarrow Ag_2O + H_2O \quad (1)$$

This leads to a decrease in OH^- available for complex formation, as Ag^+ more readily forms complexes. In addition, due to the larger size of Ag, it may cover or disrupt the crystal structure of ZnO, increasing lattice strain and reducing the crystallinity of the hexagonal ZnO phase.

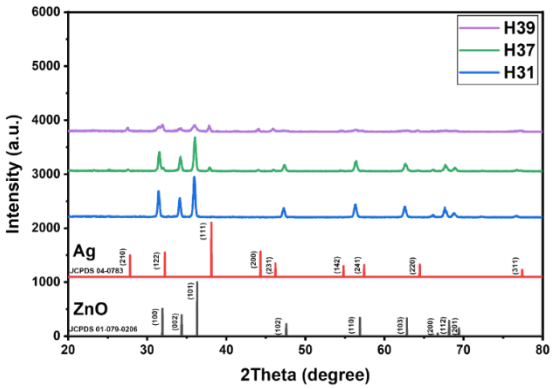


Fig. 5. The XRD patterns of Ag@ZnO samples were investigated to evaluate the effect of two types of *Dicliptera tinctoria* extracts: H37 sample (extracted with distilled water), H39 sample (extracted with a water - ethanol mixture =1 : 1), and H31 (green-synthesized ZnO nondoping Ag)

Table 2. Crystallite size, strain, and the determination factor of H37 and H39 samples determined by the Williamson-Hall method

Sample	H37		H39	
	ZnO	Ag	ZnO	Ag
Particle size (nm)	35.55	-	8.16	2.11
Microstrain (%)	1.02	-	5	33.7
R^2	0.99	-	0.66	0.43

We evaluated two *Dicliptera tinctoria* extracts: H37 (water) and H39 (a 1:1 water-ethanol mixture, identified as optimal in prior work). Based on this, the 1:1 ratio was chosen as the standard for Ag@ZnO NsMs synthesis.

3.2.2. Scanning electron microscopy results

Scanning electron microscopy (SEM) results of ZnO (H31, undoped ZnO), H37, and H39 samples are shown in Fig. 6. For the undoped ZnO sample, the crystalline particles are shown to be arranged in dense sheets with low surface porosity. SEM images of sample H37 (a ZnO nanosample doped with 7% Ag using *Dicliptera tinctoria* extract with only distilled water) show two different crystalline colors on the surface: dark and light.

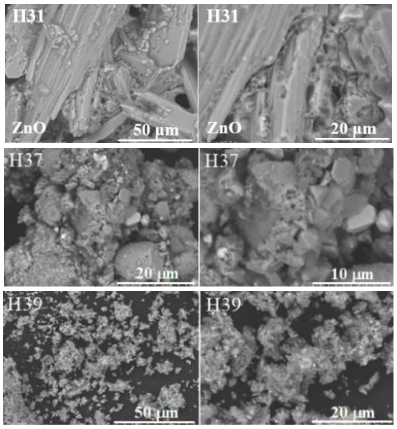


Fig. 6. SEM at different measures of 50 µm and 20 µm of H31, H37 and H39 samples

The darker color is believed to be the ZnO nano-sample, while the lighter color is believed to be the doped Ag metal present on the ZnO nano-sample. The surface of sample H37 also exhibits high porosity. Next, considering the SEM images of sample H39 (a ZnO nano-sample doped with 7% Ag using *Dicliptera tinctoria* extract with a water and ethanol mixture in a 1:1 ratio), this material also shows two different crystalline colors: dark and light. The darker crystalline color is due to ZnO nanoparticles, while the lighter crystalline color is due to the Ag metal doping on the surface of the ZnO nanomaterial. The crystal distribution on the material surface is not clustered, but evenly distributed, with high dispersion, resulting in smaller crystal size and higher porosity compared to sample H37 . The morphology revealed by the SEM images is consistent with previous reports on Ag-doped ZnO [13–15]. It can be observed that changes in the shape and

dispersion of the crystal grains among samples H31, H37, and H39 (analyzed from the SEM images in Fig. 6) are consistent with the changes in the XRD spectra (Fig. 5). Specifically, a gradual decrease in the intensity of the (101) crystal plane of hexagonal wurtzite ZnO is observed from sample H31 to H37 to H39, along with the appearance and gradual increase of the (111) peak corresponding to face-centered cubic (fcc) Ag from sample H37 to H39.

3.2.3. Diffuse reflectance spectroscopy results

The diffuse reflectance spectroscopy (DRS) spectra of the Ag@ZnO and undoped ZnO samples are shown (analyzed based on the solid-state UV-Vis spectra of the corresponding nanopowders). The band gap energy of the samples was determined from the derivative of these spectra (which was previously analyzed by our group). The results are compiled in Table 3. Based on Table 3, it can be seen that the Eg of the Ag@ZnO sample was narrower than that of the undoped ZnO sample. This finding is also consistent with the results reported in the literature [13-15].

Table 3. The band gap energy of the samples

Samples [Ref.]	**Eg (eV)**
undoped ZnO [in our earlier work]	3.23
Ag@ZnO [This word]	3.03
Pure ZnO; Ag-ZnO 6% [Ref.13]	3.14; 2.88
Pure ZnO; ZnO/Ag 10% [Ref.15]	3.07; 3.03

3.2.4. Photocatalytic efficiency

As shown in Fig. 7, the MB degradation efficiency of sample H39 reached 100% within 60 min, significantly outperforming sample H37, which achieved only 91.11% after 90 min.

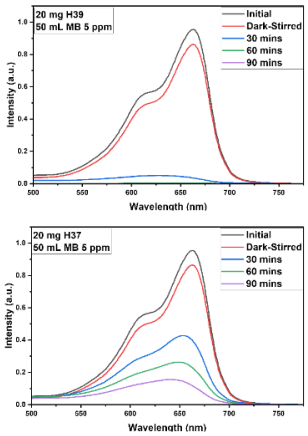


Fig. 7. Photocatalytic degradation efficiency of the Ag@ZnO materials: H39 sample and H37 sample

When comparing H37 and H39 samples, several questions arise. The crystallinity of sample H39 appears improved relative to H37, yet the hexagonal ZnO structure in H39 seems partially collapsed. A plausible explanation is that using ethanol in the *Dicliptera tinctoria* extract increases the content of polyphenols, tannins, and flavonoids due to the solvent's solubility properties [16,17]. Consequently, –OH and $–COO^-$ groups strongly interact with Zn^{2+}, coating the ZnO nanoparticles and giving the appearance of structural collapse. In contrast, Ag^+ does not strongly interact with –OH or $–COO^-$, and its large atomic mass enables strong X - ray scattering. Additionally, the coverage of –OH and $–COO^-$ groups on Ag is negligible. The enhanced peak intensity of Ag in H39 indicates improved crystallinity of Ag when the extract contains a higher amount of –OH and $–COO^-$ groups.

3.3. The Ag@ZnO Sample with the Best Efficiency was Replicated for Further Studies

To evaluate material uniformity, two additional samples (H40 and H41) were prepared using the same procedure as H39, aiming for similar photocatalytic efficiency values at corresponding time intervals. The reaction rate constants and degradation efficiencies of H39, H40, and H41 samples all reached 100% and showed uniformity after 60 minutes of photocatalysis. Thus, this experiment demonstrates the relative stability of Ag@ZnO NsMs in the degradation of MB dye solution (Fig. 8).

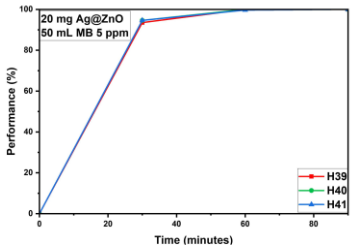


Fig. 8. UV-Vis results of the photocatalytic degradation efficiency of 5 ppm MB under UV light for three repeated syntheses under the conditions of H39 sample, namely H39, H40, and H41 samples

3.4. Investigation of Photocatalytic Degradation with Different MB Dye Solution Concentrations

Since superior photocatalytic efficiency was achieved with a MB solution of 5 ppm, further experiments were conducted on the photocatalytic degradation of MB at two higher concentrations of 10 ppm and 15 ppm under ultraviolet irradiation for 3 hours. The UV-Vis results of MB degradation at two concentrations of 10 ppm and 15 ppm are presented in Fig. 9. In the Fig. 9, it can be observed that the adsorption of Ag@ZnO NsMs is negligible (around 5%). After 180 minutes of illumination, the brown coloration of the solution almost completely disappears, indicating the superior degradation ability of MB (10 ppm) by H39 sample. And when the MB concentration is increased to 15 ppm, the adsorption by the material remains negligible (approximately 1%), and after 180 minutes of illumination, the maximum absorption peak still retains an intensity of about out of 2.2. This demonstrates that the material can still degrade

MB effectively at higher concentrations. However, the increased density of dissolved molecules in the same solution volume can lead to excessive coverage of the Ag@ZnO NsMs, hindering light access. Moreover, after repeated degradation cycles, the material may experience a limited lifespan, which can affect the efficiency in subsequent degradation processes. Table 4 shows the kinetic parameters, correlation coefficient, and degradation efficiency for two different MB concentrations. For 10 ppm MB, the correlation coefficient R^2 is 0.93, the rate constant k is 0.0306 min^{-1}, and the degradation efficiency reaches 99.76% after 180 minutes of illumination.

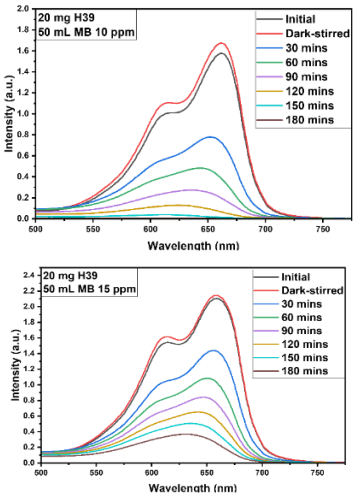


Fig. 9. The results of MB degradation efficiency for 10 ppm and 15 ppm under UV light (using H39 sample)

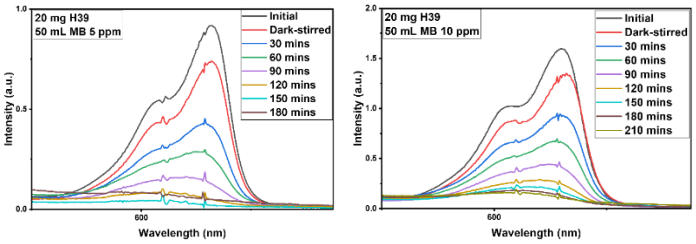
Table 4. First-order kinetic curves of H39 sample for the photocatalytic of MB solution at 10 ppm and 15 ppm

Sample	**(20 mg Ag@ZnO + 50 mL MB of 5 ppm)**	
	H39, MB 10 ppm	H39, MB 15 ppm
Kinetic equation	y=0.0306x + 0.4055	y=0.0093x + 0.0728
R^2	0.93	0.99
Efficiency (%)	99.76	82.71

For 15 ppm MB, R^2 is 0.99, k is 0.0093 min^{-1}, the efficiency is 82.71% after 180 minutes of illumination, indicating that the photocatalytic efficiency gradually decreases inversely with the MB molecular density. Thus, as the concentration of MB increases, the photocatalytic efficiency of Ag@ZnO NsMs decreases inversely with MB concentration.

3.5. Investigation of the Photocatalytic Efficiency under Visible Light Irradiation

With the aim of applying the catalyst under sunlight, after conducting investigations under UV light, we further evaluated its photocatalytic performance under visible light irradiation. In the visible-light photocatalytic experiments, two concentrations of MB, 5 ppm and 10 ppm, were selected. The photocatalytic efficiency of H39 sample under visible light irradiation with MB dye solution concentrations of 5 ppm and 10 ppm was showed in Fig. 10a and Fig. 10b. As can be seen, under the condition of 5 ppm MB degradation under visible light irradiation (Fig. 10a), after 120 minutes, the characteristic peak of MB disappeared from the spectrum, indicating that the Ag@ZnO NsMs performed very well under visible light. Some sharp or concave features may be attributed to slight optical interference or other external factors. When the MB concentration was increased to 10 ppm (Fig. 10b), after 210 minutes, the characteristic peak of MB was still observable. This suggests that increasing the dye concentration leads to a higher molecular density in the solution, reducing the number of photons available to the Ag@ZnO catalyst, thereby decreasing the generation of electron - hole pairs. Simultaneously, the higher MB concentration can block active sites and reduce reaction efficiency. From Fig. 10a and Fig. 10b, the maximum absorption peak of MB tends to shift toward shorter wavelengths, which can be explained by the breaking of bonds within the MB molecular framework, leading to a decrease in the π - bond length [18]. Additionally, the formation of intermediate products with less conjugated structures, the reduced molecular aggregation, and changes in the solution environment also contribute to this observed blue shift. Based on the UV-Vis results of MB degradation shown in Fig. 10, we analyzed the data using a pseudo-first-order kinetic model to determine the reaction rate constant [19] (Table 5).



(a) **(b)**

Fig. 10. The photocatalytic efficiency of H39 sample under visible light irradiation with MB 5 ppm (a), 10 ppm (b)

Table 5. Reaction rate constant (k), degradation efficiency, and correlation coefficient (R^2) of H39 sample under visible light irradiation [19].

Sample	k (min^{-1})	Efficiency (%)	R^2
H39, MB 5 ppm	0.022	98.12	0.93
H39, MB 10 ppm	0.012	92.52	0.94

The R^2 values for MB concentrations of 5 ppm and 10 ppm were 0.93 and 0.94, respectively. This is indicating that the assumed kinetic model fits the experimental data well. The rate constant k for MB at 10 ppm decreased by a factor of 1.83 compared to 5 ppm, highlighting the significant influence of MB concentration. After 180 minutes of illumination, the degradation efficiency for MB at 5 ppm reached 98.12%, while after 210 minutes of illumination, the efficiency for MB at 10 ppm reached 92.52%. These results demonstrate the excellent performance of the green-synthesized Ag@ZnO NsMs in degrading MB solution.

In previous experiments, our group fabricated a pure ZnO control sample using a process identical to that in Fig. 2, but using only the $Zn(NO_3)_2$ precursor and *Dicliptera tinctoria* extract, without $AgNO_3$. Similarly, a pure Ag control sample was fabricated using the same process, but using only the $AgNO_3$ precursor and *Dicliptera tinctoria* extract, without $Zn(NO_3)_2$. Table 6 presents the photocatalytic degradation results of the 10 ppm MB dye solution for various samples, including: the control samples (pure Ag, pure ZnO, and photolysis under visible light from a 250W Osram lamp), the Ag@ZnO sample (from this study), and the ZnO-Ag samples from references [14, 15].

Table 6. The results of the photocatalytic degradation efficiency of 10 ppm MB dye solution by various samples, including control samples (blank samples such as Ag, ZnO, and visible light irradiation only from an Osram 250W lamp), the Ag@ZnO sample (from this study), the pure ZnO, and the ZnO-Ag samples (according to Ref. [13-15])

Samples / 10ppm MB dye solution	Fabrication parameters: Method, Crystal size, Particle size, Photocatalytic efficiency for dye degradation, Time of irradiation, The utilized light source	Photocatalytic efficiency in the first cycle	Photocatalytic efficiency in the 2nd cycle
ZnO [our previous work]	Green method using *Dicliptera tinctoria* extract, Crystal size (39.28 nm), 57.82% for photocatalytic degradation of MB 10ppm in 210 min irradiation, using a 250W Osram lamp (visible light)	53.06%	-
Ag [our previous work]	Green method using *Dicliptera tinctoria* extract, Crystal size (~15 nm), 99.24% for photocatalytic degradation of MB 10ppm in 210 min irradiation, using a 250W Osram lamp (visible light)	97.25%	-
Visible light of 250W lamp	~8% for photocatalytic degradation of MB 10ppm in 210 min irradiation, using a 250W Osram lamp (visible light)	~6%	-
Ag@ZnO [This work]	Green method using *Dicliptera tinctoria* extract, Crystal size (8.16 nm), 92.52% for photocatalytic degradation of MB 10ppm in 210 min irradiation, using a 250W Osram lamp (visible light)	90.86%	-
Ag-ZnO 6% ZnO NPs [Ref.13]	Co-precipitation method, Ag-ZnO 6% sample: Crystal size (22.5 nm), SEM (65 nm), 77.7% for photocatalytic degradation of MO 10ppm in 120 min irradiation, using a 100W Philips lamp (visible light); ZnO sample: Crystal size (27.0 nm), SEM (85 nm), 49.3% for photocatalytic degradation of MO 10ppm in 120 min irradiation	-	-
2% Ag-ZnO 8% Ag-ZnO NPs [Ref.14]	Geen method using Potato peels extract, 2% Ag-ZnO sample: Spherical size (7-12 nm), 96% for photocatalytic degradation of MB 5ppm and 50-60% for photocatalytic degradation of MB 10ppm in 80-120 min irradiation, using a 250W visible lamp; 8% Ag-ZnO sample: Spherical size (15-25 nm), 85% for photocatalytic degradation of MB 5ppm within 80-120 min irradiation, using a 250W visible lamp	Slight decrease of 6% in degradation of MB	The MB degradation rate showed a further slight decrease of 4%
ZnO/Ag 10% ZnO NCs [Ref.15]	Geen method using Pineapple peel extract, ZnO/Ag 10% sample: Crystal size (18.12 nm), SEM (126 nm), 41.29% for photocatalytic degradation of MB 10ppm affter 120 min irradiation, using four UV-C lapms (8 watts); ZnO sample: Crystal size (16.35 nm), SEM (254 nm), 12.96% for photocatalytic degradation of MB 10ppm	-	-

Note:MB, Methyl orange (MO), Nanoparticles (NPs), Nanocomposites (NCs)

As shown in Table 6, the blank sample (exposed only to the visible light of the 250W Osram lamp without a catalyst) exhibited almost no photocatalytic activity, with MB degradation reaching only 6–8% after 210 minutes of illumination. The pure ZnO control sample achieved a low degradation efficiency of about 50–60% after 210 minutes. In contrast, the pure Ag control sample showed a high photocatalytic efficiency of 99.24% after 210 minutes. And after 1 recycling test, its degradation efficiency decreased slightly by 2%. Meanwhile, the Ag@ZnO sample exhibited stable photocatalytic performance, with a performance loss of only about 1.79% after 1 recycling cycle. Overall, the photocatalytic performance of our sample is competitive compared to other previous studies [13-15].

4. Conclusion

In summary, the green-synthesized Ag@ZnO material exhibits well-defined crystal phases of hexagonal ZnO and face-centered cubic Ag, as confirmed by XRD analysis. Through the investigation, a silver doping level of 7% (molar ratio relative to Zn) was found to provide the optimal dye degradation efficiency of 91.11% (using water in the extraction process). Using a water-alcohol mixture (1:1 ratio) in the extraction process increased the content of organic compounds, thereby partially covering the ZnO surface; however, this did not negatively affect the results. On the contrary, the Ag@ZnO sample achieved a complete MB degradation efficiency of 100% after 60 minutes of UV illumination. After three repeated syntheses, the photocatalytic efficiency remained consistent, demonstrating the material's stability. Evaluating the photocatalytic performance under visible light is important for practical applications. In these tests, with MB concentrations of 5 ppm and 10 ppm, the degradation efficiencies reached 98.12% and 92.52%, respectively, after 180 and 210 minutes of illumination.

Acknowledgments

The authors thank the C9-110 Optics and Optoelectronics Laboratory. The authors thank the C1 401 Photocatalytic, Adsorption, and Green Energy Materials Laboratory. The authors express their sincere gratitude for the valuable technical support and the provision of facilities by the Ceramic Materials Research and Development Laboratory throughout the course of the research. This research is funded by Hanoi University of Science and Technology (HUST) under project number T2025-PC-095.

References

[1] J. Shamshad, R. Ur Rehma, Innovative approaches to sustainable wastewater treatment: A comprehensive exploration of conventional and emerging technologies, Environmental Science: Advances, vol. 4, no. 2, pp. 189–222, Nov. 2024. https://doi.org/10.1039/D4MA00136B

[2] J. Singh, T. Dutta, Ki-Hyun Kim, M. Rawat, P. Samddar, and Pawan Kumar, 'Green' synthesis of metals and their oxide nanoparticles: Applications for environmental remediation, Journal of Nanobiotechnology, vol. 16, Oct. 2018, Art. no. 84. https://doi.org/10.1186/s12951-018-0408-4

[3] L.S. Reddy Yadav, S. Pratibha, K. Manjunath, M. Shivanna, T. Ramakrishnappa, N. Dhananjaya, and G. Nagaraju, Green synthesis of Ag-ZnO nanoparticles: Structural analysis, hydrogen generation, formylation and biodiesel applications, Journal of Science: Advanced Materials and Devices, vol. 4, iss. 3, pp. 425–431, Sep. 2019. https://doi.org/10.1016/j.jsamd.2019.03.001

[4] M. F. Abdel Messih, M. A. Ahmed, Ayman Soltan, and Samy Sobhy Anis, Synthesis and characterization of novel Ag/ZnO nanoparticles for photocatalytic degradation of methylene blue under UV and solar irradiation, Journal of Physics and Chemistry of Solids, vol. 135, Dec. 2019, Art. no. 109086. https://doi.org/10.1016/j.jpcs.2019.109086

[5] Martin Medina-Acosta, Manuel J. Chinchillas-Chinchillas, Horacio E. Garrafa-Gálvez, Caree A. Garcia-Maro, Carlos A. Rosas-Casarez, Eder Lugo-Medina, Priscy A. Luque-Morales, and Carlos A. Soto-Robles, Photocatalytic degradation of four organic dyes present in water using ZnO nanoparticles synthesized with green synthesis using Ambrosia ambrosioides leaf and root extract, Processes, vol. 12, iss. 11, Art. no. 2456, Nov. 2024. https://doi.org/10.3390/pr12112456

[6] Sadia Aroob, Sónia A. C. Carabineiro, Muhammad Babar Taj, Ismat Bibi, Ahmad Raheel, Tariq Javed, Rana Yahya, Walla Alelwani, Francis Verpoort, Khanita Kamwilaisak, Saleh Al-Farraj, and Mika Sillanpää, Green synthesis and photocatalytic dye degradation activity of CuO nanoparticles, Catalysts, vol. 13, iss. 3, Feb. 2023, Art. no. 502. https://doi.org/10.3390/catal13030502

[7] Le Manh Cuong, Le Cong Chung, Tran Thanh Thai, and Luu Thi Lan Anh, Investigation of the Cam leaf extraction process oriented to synthesize silver nanoparticles (Ag NPs), Vietnam Journal of Catalysis and Adsorption, vol. 12, no. 1, pp. 85–90, Mar. 2023. https://doi.org/10.51316/jca.2023.014

[8] S. Shahzadi, S. Fatima, Q. ul Ain, Z. Shafiqa, and M. R. S. A. Janjua, A review on the green synthesis of silver nanoparticles (SNPs) using plant extracts: a multifaceted approach in photocatalysis, environmental remediation, and biomedicine, RSC Advances, vol. 15, iss. 5, pp. 3858–3903, Jan. 2025. https://doi.org/10.1039/D4RA07519F/v3/response1

[9] Sarika Singh, Natural sunlight driven photocatalytic performance of Ag/ZnO nanocrystals, Materialstoday Communications, vol. 33, Dec. 2022, Art. no. 104438. https://doi.org/10.1016/j.mtcomm.2022.104438

[10] P. Kumari, N. Bahadur, L. Kong, L. A. O'Dell, A. Merenda, and L. F. Dumée, Engineering Schottky-like and heterojunction materials for enhanced photocatalysis performance - a review, Materials Advances, vol. 3, no. 5, pp. 2309–2323, Jan. 2022. https://doi.org/10.1039/D1MA01062J

[11] José Vulfrano González-Fernández, Diego David Pinzón-Moreno, Antony Alexander Neciosup-Puican, and María Verónica Carranza-Oropeza, Green method, opticaland structural characterization of ZnO nanoparticles synthesized using leaves extract of *M. oleifera*, Journal Renewable Materials, vol. 10, no. 3, pp. 834–846, Sep. 2022. https://doi.org/10.32604/jrm.2022.017377

[12] Amrut S. Lanje, Satish J. Sharma, and Ramchandra B. Pode, Synthesis of silver nanoparticles: A safer alternative to conventional antimicrobial and antibacterial agents, Journal of Chemical and Pharmaceutical Research, vol. 2, iss. 3, pp. 478–483, 2010, [Online]. Available: www.jocpr.com

[13] Atif Hussain, Shamaila Fiaz, Abdullah Almohammedi, and Aqsa Waqar, Optimizing photocatalytic performance with Ag-doped ZnO nanoparticles: Synthesis and characterization, Heliyon, vol. 10, iss. 15, Aug. 2024, Art. no. e35725. https://doi.org/10.1016/j.heliyon.2024.e35725

[14] Fahad A. Alharthi, Abdulaziz Ali Alghamdi, Nabil AI-Zaqri, Hamdah S. Alanazi, Amjad Abdullah Alsyahi, Adel EI Marghany, and Naushad Ahmad, Facile one pot green synthesis of Ag-ZnO nanocomposites using potato peeland their Ag concentration dependent photocatalytic properties, Scientific Reports, vol. 10, Nov. 2020, Art. no. 20229. https://doi.org/10.1038/s41598-020-77426-y

[15] Ari Sulistyo Rini, Rahmi Dewi, Jasril, Tessa Marshanda, Yolanda Rati, and Yan Soerbakti, Synthesis and characterisation of ZnO/Ag nanocomposites prepared via green method using pineapple peel extract for photocatalytic enhancement in degrading methylene blue dye solutions, Journal of Physical Science, vol. 34, no. 2, pp. 59–73, Aug. 2023. https://doi.org/10.21315/jps2023.34.2.5

[16] Panikchar Wichayapreechar, Ranit Charoenjittichai, Anchalee Prasansuklab, Pimchanok Charoongchit, and Eakkaluk Wongwad, Evaluation of biological activities and cytotoxicity of peristrophe bivalvis (L.) Merr extracts and investigation of its Novel natural active ingredient-loaded nanoemulsion and stability assessment, Cosmetics, vol. 12, iss. 3, May 2025, Art. no. 92. https://doi.org/10.3390/cosmetics12030092

[17] Ketut Agus Adrianta, Bagus Komang Satriyasa, Desak Made Wihandani, I Made Jawi, The antioxidant capacity of Peristrophe bivalvis (L.) Merr. as natural-based nephroprotection, Traditional Medicine Journal, vol. 26, pp. 35–41, 2021. https://doi.org/10.22146/mot.53861

[18] Yi Hsuan Chiu, Tso Fu Mark Chang, Chun Yi Chen, Masato Sone, and Yung Jung Hsu, Mechanistic insights into photodegradation of organic dyes over photocatalysts, Catalysts, vol. 9, iss. 5, Apr. 2019, Art. no. 430. https://doi.org/10.3390/catal9050430

[19] H. D. Tran, D. Q. Nguyen, P. T. Do, and U. N. P. Tran, Kinetics of photocatalytic degradation of organic compounds: A mini-review and new approach, RSC Advances, vol. 13, iss. 25, pp. 14012–14034, Jun. 2023. https://doi.org/10.1039/D3RA01970E